

CHARACTERIZATION OF THE LAMELLAR STRUCTURE IN Ti-RICH TiAl COMPOUNDS BY HIGH-RESOLUTION ELECTRON MICROSCOPY AND COMPUTER IMAGE SIMULATION

H. INUI AND M. YAMAGUCHI

Department of Metal Science and Technology, Kyoto University
Sakyo-ku, Kyoto 606, Japan

ABSTRACT

Characterization of the lamellar structure in Ti-rich TiAl compounds has been made by high-resolution electron microscopy coupled with the computer simulation of HREM images. The lamellar boundaries between TiAl ordered domains as well as those between TiAl and Ti₃Al were characterized on an atomistic scale. Boundaries between TiAl domains are atomistically flat except for the presence of ledges of two (111)_{TiAl} planes high and in most cases, contain no Ti₃Al plates. Boundaries between TiAl and Ti₃Al are also atomistically flat and perfectly coherent but contain somewhat more ledges of two (111)_{TiAl} planes high. At interfaces between TiAl and Ti₃Al, the atomic rows composed of Ti atoms only are aligned across the interface between the two phases.

1. INTRODUCTION

In recent five years, there has been enormous increase in the research and development activity on titanium aluminides, particularly on TiAl-based compounds as potential light-weight high-temperature structural materials [1-4]. Since the intermetallic compound TiAl has a composition range primarily on the Al-rich side of the stoichiometry, Ti-rich TiAl compounds exhibit a two phase microstructure composed of the TiAl(γ) phase and a small volume fraction of the Ti₃Al(α_2) phase. Recent research interest has been focused on such two-phase Ti-rich TiAl compounds rather than on single-phase Al-rich TiAl compounds because of the better ductility and toughness of the two-phase Ti-rich TiAl compounds at ambient temperature [5,6]. It is characteristic of the two-phase Ti-rich TiAl compounds that they exhibit the lamellar structure consisting of the twin-related TiAl and the Ti₃Al phases with the orientation relationship of $\{111\}_\gamma // (0001)_{\alpha_2}$ and $\langle 1\bar{1}0 \rangle_\gamma // \langle 11\bar{2}0 \rangle_{\alpha_2}$ [7]. Although the lamellar structure has been believed to be closely related to the ductility and toughness of the two-phase Ti-rich TiAl compounds, it is not clear at present how the lamellar structure is related to those mechanical properties. Recent microstructural studies have established that six different types of ordered domains exist in the TiAl phase in the lamellar structure [8-12]. Since dislocations will meet and interact with domain boundaries in the TiAl phase as well as interphase boundaries between TiAl and Ti₃Al in the course of deformation of Ti-rich TiAl compounds, the deformation behavior of the compounds is affected by the presence of ordered domains in the TiAl phase. It is, therefore, indispensable to investigate the TiAl/Ti₃Al lamellar structure for the better understanding of the deformation behaviour of the two-phase Ti-rich TiAl compounds.

In the present study, characterization of the lamellar structure of two-phase Ti-rich TiAl compounds has been made on an atomistic scale by

high-resolution microscopy (HREM) coupled with computer simulation of HREM images. Energies of various TiAl/Ti₃Al interfaces were estimated on the basis of a hard sphere model and discussed based on the observed frequency.

2. EXPERIMENTAL PROCEDURES

2.1. HREM observations

Ti-rich TiAl polysynthetically twinned (PST) crystals, which contain a single grain with the TiAl/Ti₃Al lamellar structure, were grown by a floating zone method, from the master ingot with a composition of Ti-49.3at.%Al. Slices, approximately 300 μm in thickness, were cut parallel to the {110} planes, which are perpendicular to the (111) lamellar boundary planes, to observe the lamellar boundaries edge-on. These slices were mechanically polished to about 100 μm in thickness, and then finished by a standard double-jet polishing method for HREM observations. HREM observations were carried out using a JEM-4000EX electron microscope operated at 350 kV to prevent severe radiation damage during observations. On HREM observations, through-focus series were taken at various interfaces using a 12 nm⁻¹ radius objective aperture and focus increments of 3.6 nm.

2.2. Computer simulations of HREM images

High resolution electron microscope images were calculated by a multi-slice method using a JEM-1000 multi-slice simulation software. Among the parameters involved in the simulations, the accelerating voltage of electrons (E), the spherical aberration constant (C_s) and the defocus of the objective lens (Δf) are the most important ones, since the contrast of high-resolution images (phase contrast) is determined mainly by the contrast transfer function [13] shown in eq.(1).

$$\gamma = \frac{\pi}{2\lambda} (C_s \alpha^4 + 2 \Delta f \alpha^2) \quad \dots (1)$$

where λ and α are the wave length of electrons and the objective lens aperture angle, respectively. The other parameters involved in the simulations were the fluctuation of the accelerating voltage (ΔE), the chromatic aberration constant (C_c), and the crystal thickness (t). In the simulation of high-resolution images, several parameters such as E=350 kV, ΔE=0.7 eV, C_s=1.0 mm, C_c=1.7 mm and α=0.5 mrad were fixed at the constant values specific for the JEM-4000EX electron microscope, while the crystal thickness and the defocus of the objective lens were systematically changed. Image simulations were carried out for the images of TiAl with the incident beam parallel to [110] and [011] and of Ti₃Al with the incident beam parallel to [1120]. Furthermore, images of two types of TiAl_{[110]0}/Ti₃Al_[1120] interfaces were calculated and compared with the observed images.

3. RESULTS

3.1. The lamellar structure of Ti-rich TiAl compounds

The lamellar structure of Ti-rich TiAl compounds consists of the twin-related TiAl(γ) phase and a small volume fraction of the Ti₃Al(α₂) phase.

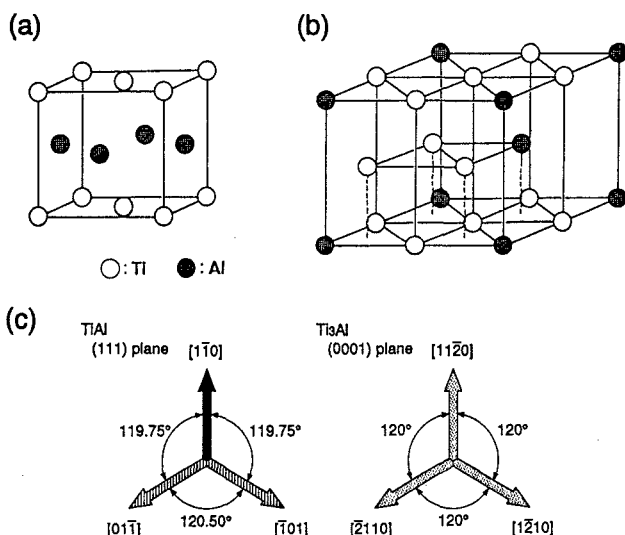


Fig.1 The crystal structure of (a) TiAl and (b) Ti_3Al , and the orientation relationship between TiAl and Ti_3Al in the lamellar structure is shown in (c).

TiAl possesses the tetragonal $L1_0$ structure ($a=0.400$ nm and $c=0.406$ nm ; $c/a=1.015$) while Ti_3Al has the hexagonal DO_{19} structure ($a=0.577$ nm and $c=0.462$ nm ; $c/a=0.801$) [4], as respectively shown in Figs.1(a) and (b). The orientation relationship between the two phases in the lamellar structure has been established to be $\{111\}_\gamma // (0001)_{\alpha_2}$ and $\langle 1\bar{1}0 \rangle_\gamma // \langle 11\bar{2}0 \rangle_{\alpha_2}$ [7], as shown in Fig.1(c). Since three $\langle 11\bar{2}0 \rangle$ directions on the basal plane of the Ti_3Al phase are all equivalent while the $[1\bar{1}0]$ direction and the other two $\langle 01\bar{1} \rangle^*$ directions on the (111) plane of the TiAl phase are not equivalent to each other, there are six possible orientations for the $[1\bar{1}0]$ direction of the TiAl phase with respect to $\langle 11\bar{2}0 \rangle$ directions of the Ti_3Al phase, i.e.,

$$[1\bar{1}0]_\gamma // [11\bar{2}0]_{\alpha_2}, [1\bar{1}0]_\gamma // [1\bar{2}10]_{\alpha_2}, [1\bar{1}0]_\gamma // [2110]_{\alpha_2} \quad \dots \quad (2)$$

and

$$[1\bar{1}0]_\gamma // [11\bar{2}0]_{\alpha_2}, [1\bar{1}0]_\gamma // [1\bar{2}10]_{\alpha_2}, [1\bar{1}0]_\gamma // [2110]_{\alpha_2} \quad \dots \quad (3)$$

where $//$ and $//$ mean parallel and antiparallel, respectively. Thus, six different types of ordered domains are formed in the TiAl phase corresponding to these six possible orientation variants. If we describe the stacking sequence of the (111) close-packed planes of the three TiAl ordered domains corresponding to eq.(2) as $\dots ABCABC\dots$, that of the other three TiAl ordered domains corresponding to eq.(3) can be described as $\dots CBACBA\dots$, i.e., the stacking sequence is reversed. If the slight tetragonality of the TiAl phase is ignored, orientation relationships between the two neighbouring TiAl ordered domains can be described as follows,

$$(a) [1\bar{1}0] // [1\bar{1}0], (b) [1\bar{1}0] // [\bar{1}01], (c) [1\bar{1}0] // [01\bar{1}] \quad \dots \quad (4)$$

and

$$(a) [1\bar{1}0] // [1\bar{1}0], (b) [1\bar{1}0] // [\bar{1}01], (c) [1\bar{1}0] // [01\bar{1}] \quad \dots \quad (5)$$

*The mixed notations $\{hkl\}$ and $\langle uvw \rangle$ are used to differentiate the first two indices from the third one which does not play the same role as the first two because of the tetragonality of TiAl with the $L1_0$ structure.

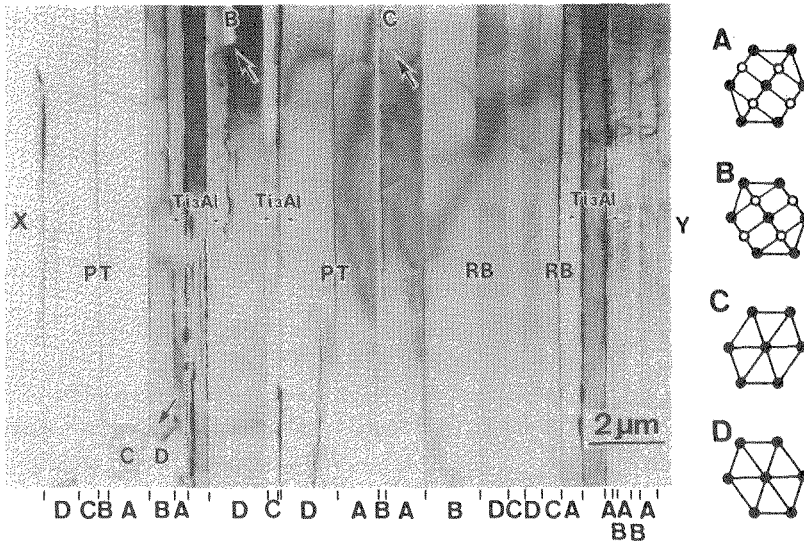


Fig.2 The lamellar structure of Ti-rich TiAl PST crystals [12].

In the case of $[1\bar{1}0] \parallel [1\bar{1}0]$, a translation order-fault boundary is formed, otherwise no boundary is produced. However, we have not observed this type of boundaries. For the other two parallel cases in eq.(4), which are equivalent to each other, a 120° -rotational order fault boundary is formed. In this case, the c-axes of the two neighbouring domains are always perpendicular to each other and the stacking sequence of the (111) planes is preserved across the domain boundary.

In the case of $[1\bar{1}0] \parallel [1\bar{1}0]$, the two neighbouring domains have the (111)[11 $\bar{2}$] true-twin relation. For the other two antiparallel cases in eq.(4), which are again equivalent to each other, pseudotwins are formed. In these pseudotwin cases, the $[1\bar{1}0]$ direction of the twin domain is rotated by 60° with respect to the $[1\bar{1}0]$ direction of the matrix domain on the (111) planes and the stacking sequence of the (111) planes is reversed across the domain boundaries. Thus, five types of orientation relationships are possible between two neighbouring TiAl ordered domains.

The difference in the crystal orientation among TiAl ordered domains can be distinguished by taking a selected area electron diffraction (SAED) pattern from each domain along $\langle 1\bar{1}0 \rangle$ parallel to the lamellar boundaries, since superlattice reflections as well as fundamental reflections (corresponding to those of a f.c.c. structure) occur in the $\langle 1\bar{1}0 \rangle$ net SAED patterns while in the $\langle 01\bar{1} \rangle$ patterns, only fundamental reflections occur.

A typical microstructure of as-grown PST crystals viewed along the $\langle 1\bar{1}0 \rangle, \langle 11\bar{2}0 \rangle_{a_2}$ direction is presented in Fig.2. In the right of the figure, the possible $[1\bar{1}0]$ and $\langle 01\bar{1} \rangle$ net SAED patterns are schematically illustrated in A, B and C, D, respectively. The types (A-D) of the obtained SAED patterns taken from each individual lamella on the X-Y line are depicted at the bottom of the figure. The lamellar boundaries are seen to be flat and parallel to both the (111) $_r$ and (0001) $_{a_2}$ planes in agreement with the previous studies [7-11]. As can be seen in Fig.2, each TiAl lamella has a thickness of $0.5-2 \mu\text{m}$. Ti_3Al lamellae with a thickness of about $0.5 \mu\text{m}$ are separated by some TiAl lamellae and exist every about $10 \mu\text{m}$. Between Ti_3Al lamellae, TiAl lamellae exist as ordered domains with various orientation relationships with the neighbouring domains. In most cases, the two neigh-

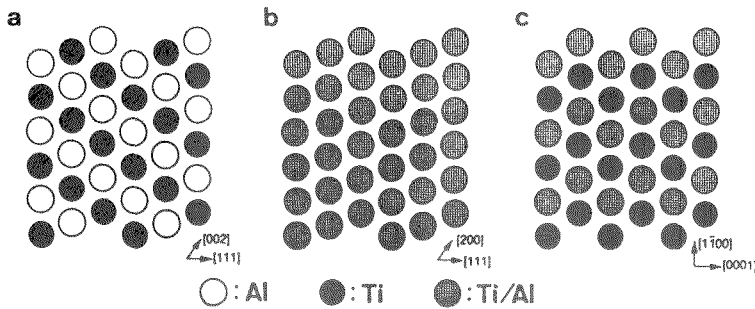


Fig.3 Schematic illustrations of atomic arrangement of (a) $\text{TiAl}_{[110]}$, (b) $\text{TiAl}_{[101]}$ ant (c) $\text{Ti}_3\text{Al}_{[1120]}$.

neighbouring TiAl domains are in true-twin relation, i.e., domains with the SAED pattern A or C border those with the pattern B or D. However, the two neighbouring TiAl domains are sometimes in pseudotwin relation as indicated by PT. Rotational order-fault boundaries are also found occasionally, as indicated by RB. These observations strongly suggest that all of the five possible orientation relationships can occur between two neighbouring TiAl ordered domains separated by the lamellar domain boundaries.

TiAl ordered domains with different orientations can also coexist within each of TiAl lamellae. The boundaries between such domains are indicated by arrows in the figure. The types of SAED patterns taken from such domains are also shown in the figure. TiAl domains with the SAED patterns A and D coexist with domains with those C and B, respectively. This indicates that TiAl domains coexisting within a TiAl lamella have the same stacking sequence of the (111) planes [10,12].

3.2. HREM images of TiAl and Ti_3Al

As described in 3.1., in TiAl, the $[1\bar{1}0]$ direction is not crystallographically equivalent to the $[10\bar{1}]$ and $[01\bar{1}]$ directions which are equivalent to each other. The atomic row along the $[1\bar{1}0]$ direction consists of either Ti or Al atoms while that along the $[10\bar{1}]$ or $[01\bar{1}]$ direction consists of Ti and Al atoms alternately occupying atomic sites on the row, as shown in Figs.3(a) and (b). Therefore, it is expected that the HREM images of TiAl taken along the $[1\bar{1}0]$ direction are different from those taken along the $[10\bar{1}]$ or $[01\bar{1}]$ direction because the atomic rows composed of Ti atoms would be imaged differently from those made up of Al atoms only. On the other hand, in Ti_3Al there are two kinds of atomic rows along the $\langle 11\bar{2}0 \rangle$ directions; the atomic rows composed of Ti atoms only and those made up of alternately arranged Ti and Al atoms, as shown in Fig.3(c). From the same reason as mentioned above, these two kinds of atomic rows could be distinguished.

Image simulations were carried out to see whether or not the atomic rows composed of Ti atoms only can be distinguished from the others for the three cases; TiAl along $[1\bar{1}0]$, TiAl along $[01\bar{1}]$ and Ti_3Al along $[11\bar{2}0]$. In the simulations, the crystal thickness was changed from 2 to 14 nm and the defocus value was systematically changed from the just focus ($\Delta f = 0$ nm) to $\Delta f = 120$ nm (under focus) through the Scherzer focus ($\Delta f \sim 40$ nm). The results obtained are illustrated in Figs.4, 5 and 6, respectively.

Fig. 4

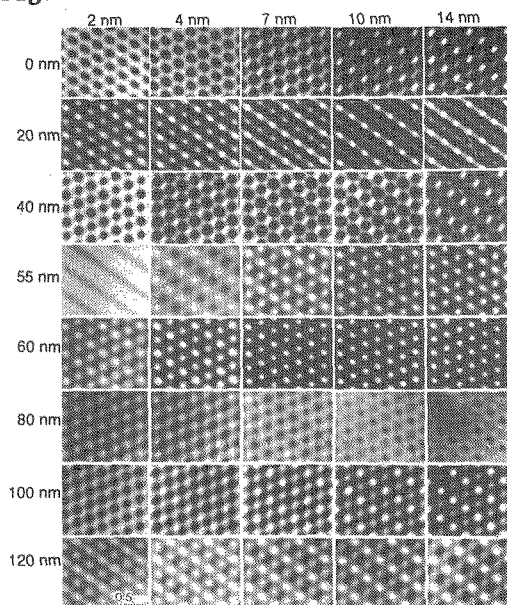


Fig. 5

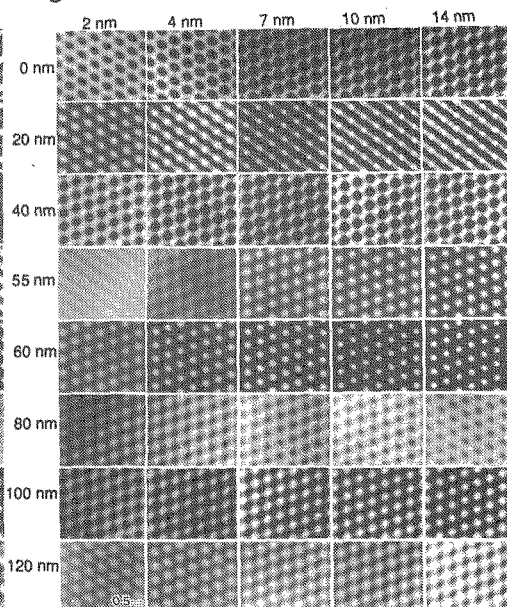


Fig. 6

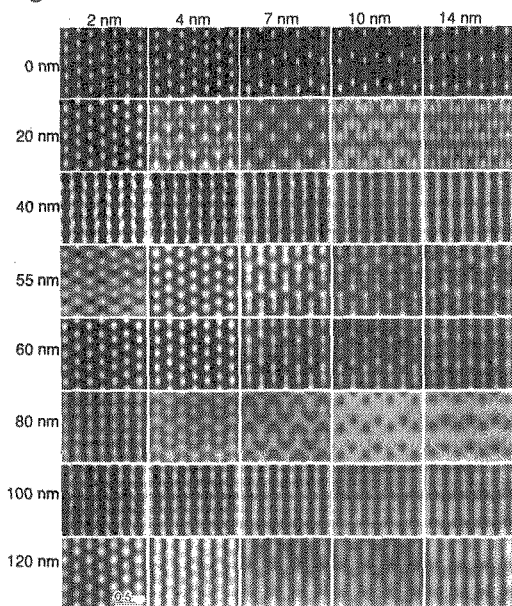


Fig.4 Calculated HREM images of $TiAl_{[11\bar{1}0]}$.

Fig.5 Calculated HREM images of $TiAl_{[01\bar{1}]}$.

Fig.6 Calculated HREM images of $Ti_3Al_{[11\bar{2}0]}$.

Figure 4 shows the calculated HREM images of TiAl along the $[1\bar{1}0]$ direction. At the Scherzer defocus value, the atomic positions are imaged as dark spots but the contrast of images are reversed at the other defocus values used, i.e., the atomic positions are imaged as bright spots. This behaviour is essentially independent on crystal thickness. It should be noted that there are two kinds of bright spots in those images; the strongly and weakly bright spots respectively corresponding to the atomic rows composed of Ti atoms only and those composed of Al atoms only. Thus, the atomic rows composed of Ti atoms only can be distinguished from those composed of Al atoms only. The calculated HREM images of TiAl along the

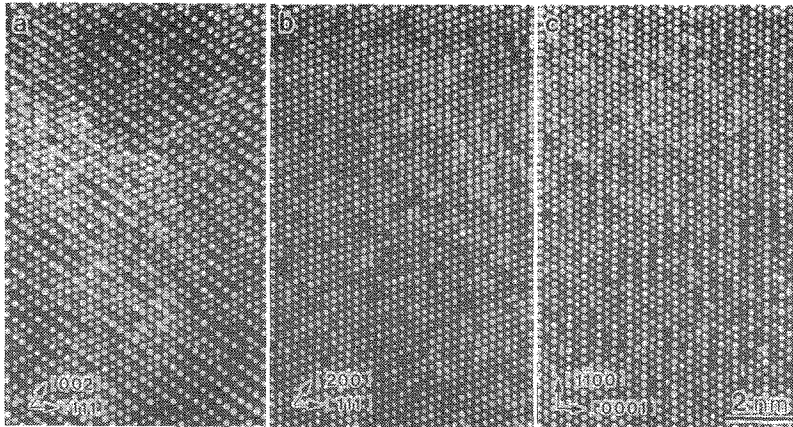


Fig.7 Typical examples of HREM images of (a) $\text{TiAl}_{[110]}$, (b) $\text{TiAl}_{[011]}$ and (c) $\text{Ti}_3\text{Al}_{[1120]} [11]$.

$[01\bar{1}]$ direction are shown in Fig.5. Again, the atomic positions are imaged as dark spots at the Scherzer defocus value and the contrast is reversed at the other defocus values used. But in this case, there is no distinction among the brightness of atomic positions. This is due to the fact that all the atomic rows along the $[01\bar{1}]$ direction of TiAl are composed of alternatively arranged Ti and Al atoms. The calculated HREM images of Ti_3Al along the $[11\bar{2}0]$ direction are shown in Fig.6. In this case, two kinds of bright spots can be seen at the defocus values of 20, 60 and 120 nm for the smaller crystal thickness, although the difference in contrast is not remarkable when compared with the case of TiAl along the $[1\bar{1}0]$ direction (Fig.4). These two kinds of bright spots, the strongly and weakly bright spots are respectively corresponding to the atomic rows composed of Ti atoms only and those composed of alternatively Ti and Al atoms.

Figures 7(a), (b) and (c) depict typical examples of experimental HREM images of TiAl taken along the $[1\bar{1}0]$ and $[01\bar{1}]$ directions and that of Ti_3Al taken along the $[11\bar{2}0]$ direction, respectively. The features observed in these HREM images are in good agreement with those of the calculated images shown in Figs.4-6.

3.3. Interfaces between TiAl ordered domains

Figures 8(a)-(c) depict schematic illustrations of possible interfaces between the twin-related TiAl ordered domains and their typical examples of HREM images are presented in figs.8(d)-(f), respectively. The features observed in the HREM images are all in consistent with those of the atomic arrangement shown in the corresponding schematic illustrations. Figures 8(a) and (d) show true (ordered) twins corresponding to the case (a) in eq.(5) while Figs.8(c) and (f) show pseudotwins corresponding to the cases (b) and (c) in eq.(5). In Figs.8(b) and (e), there is no distinction in brightness of bright spots, suggesting that all the atomic rows in the figure are composed of alternatively arranged Ti and Al atoms, that is, those along the $[01\bar{1}]$ or $[10\bar{1}]$ direction. It is, however, very difficult to judge whether this interface is that of true twins or pseudotwins only from the figure. In most cases, the interfaces between the twin-related TiAl ordered domains are atomistically flat and coherent and contain no Ti_3Al

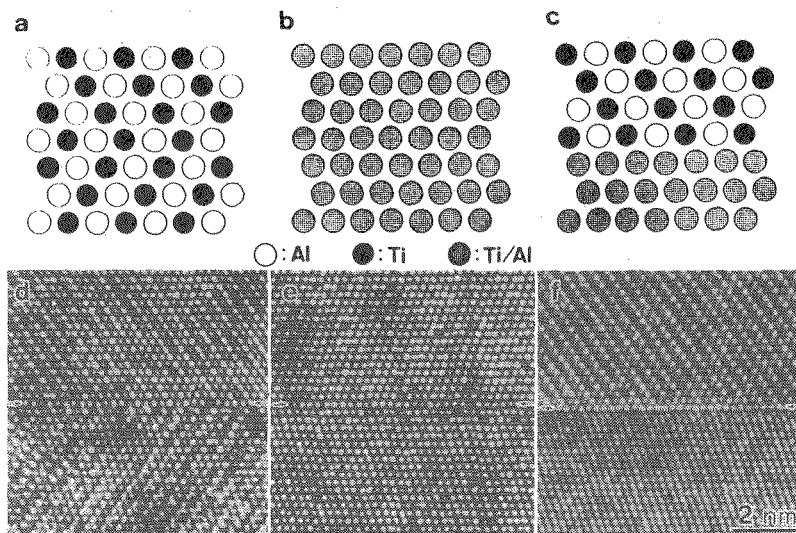


Fig. 8 Schematic illustrations of interfaces between twin-related TiAl domains; (a) $\text{TiAl}_{[110]}/\text{TiAl}_{[110]}$, (b) $\text{TiAl}_{\langle 011 \rangle}/\text{TiAl}_{\langle 011 \rangle}$ and (c) $\text{TiAl}_{[110]}/\text{TiAl}_{[011]}$. The corresponding HREM images are shown in (d)-(f), respectively [11].

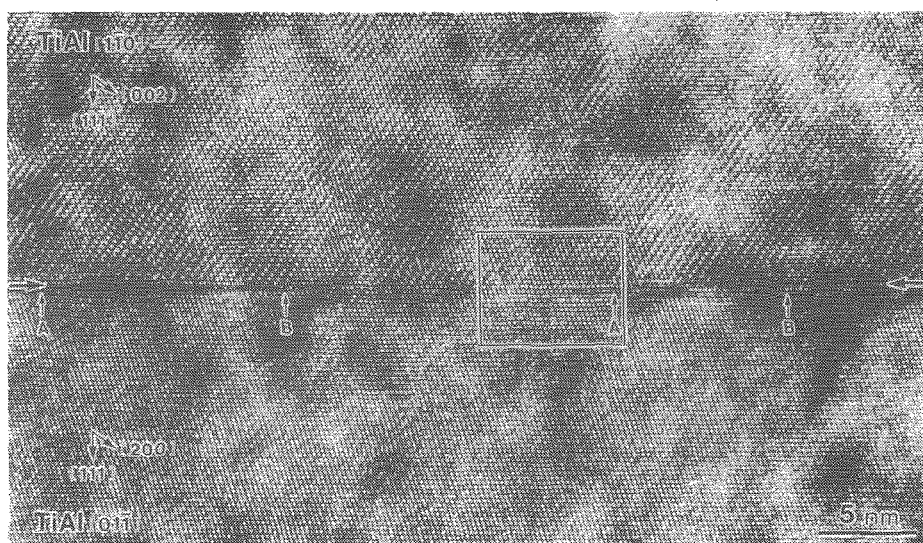


Fig. 9 HREM image of a $\text{TiAl}_{[110]}/\text{TiAl}_{[011]}$ interface of the 120° -rotational type [11].

plates.

Another type of interface between TiAl ordered domains is presented in Fig.9. In the figure, the interface is located horizontally at the center of the image and the upper and lower half are TiAl domains viewed along the $[110]$ and $[011]$ directions, respectively. In this case, these two TiAl domains are not in twin-relation but have the stacking sequence of the (111) planes. Although the interface seems atomistically very flat, there is a ledge of two atomic planes high between arrows A and B. The dark contrast associated with the ledge can be seen between arrows A and B in the image,

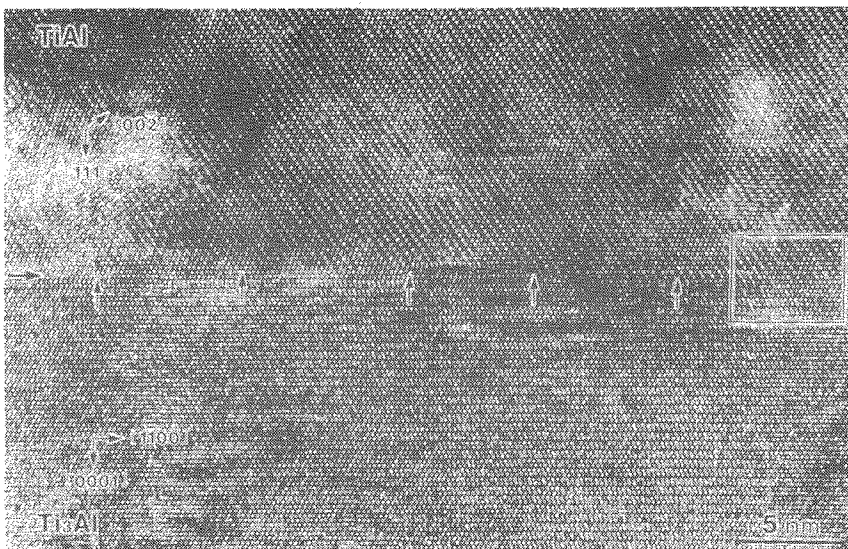


Fig.10 HREM image of a $\text{TiAl}_{[11\bar{1}0]}/\text{Ti}_3\text{Al}_{[11\bar{1}20]}$ interface $[11]$.

suggesting the presence of defects responsible for the ledge. It has been believed that a thin Ti_3Al plate is present at this type of interface to separate these two TiAl variants [8,9], since the APB energy on the $\{111\}$ planes in TiAl is considerably high. Close examination of Fig.9, however, reveals that the ...ABCABC... stacking sequence of TiAl is maintained across the interface without being disturbed by the presence of the Ti_3Al phase with the ...ABAB... stacking sequence. This indicates that at most only two layers of the Ti_3Al phase can be present at the interface. Since it is practically impossible to ascribe two layers of a certain atomic arrangement to a phase with a certain crystal structure, it can be reasonably concluded that there is no Ti_3Al plates at this interface.

3.4. Interfaces between TiAl and Ti_3Al lamellae

A typical example of HREM images of $\text{TiAl}_{[11\bar{1}0]}/\text{Ti}_3\text{Al}_{[11\bar{1}20]}$ interfaces is presented in Fig.10. The interface is located horizontally at the center of the image and the upper and lower half are TiAl and Ti_3Al , respectively. In this figure, the characteristic atomic arrangement of TiAl along the $[1\bar{1}0]$ direction is evident as the light/dark contrast among alternate (002) planes. It is evident in the figure that the interface is again flat on an atomic scale except for some ledges with two $(111)_{\text{TiAl}}$ planes high (indicated by arrows) and perfectly coherent.

In order to obtain information about the atomic structure of TiAl/ Ti_3Al interfaces, two possible model interfaces at the atomic level were constructed and these are illustrated in Figs.11(a) and (b). In Fig.11, the TiAl/ Ti_3Al interface is viewed along the $[1\bar{1}0]_{\text{TiAl}}/[1\bar{1}20]_{\text{Ti}_3\text{Al}}$ direction and is parallel to both (111) planes of TiAl and (0001) planes of Ti_3Al . The stacking sequence of these close packed planes is denoted in the figures. It should be noted here that in the model interface shown in Fig.11(a), the atomic rows composed of Ti atoms only in the TiAl and Ti_3Al phases are aligned across the interface, while not in the model interface shown in

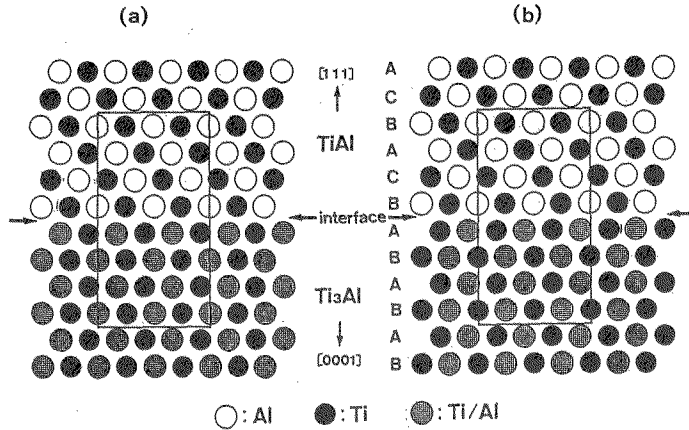


Fig.11 Model interfaces of $TiAl_{111101}/Ti_3Al_{111201}$. In (a), the atomic rows composed of Ti atoms only in $TiAl$ and Ti_3Al are aligned across the interface while not in (b) [11].

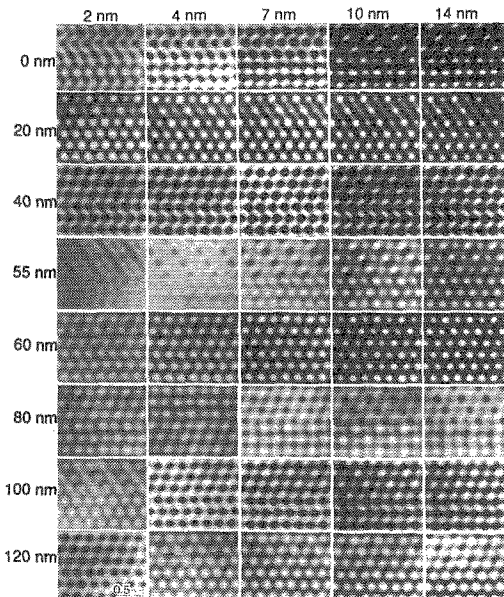


Fig.12 Calculated HREM images of the model interface (a) in Fig.11.

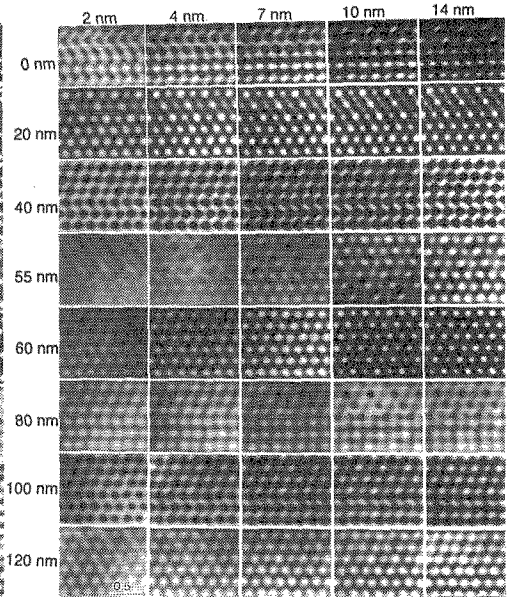


Fig.13 Calculated HREM images of the model interface (b) in Fig.11.

Fig.11(b) [11,14]. Because of the difference in atomic arrangement at the interface, one of the two model interfaces would be in the lower energy state. Since interfaces of energetically favored type must be formed on solidification, it is interesting to observe the interfaces from this point of view.

Computer simulations of HREM images were carried out for both the model interfaces, (a) and (b), using the unit cell including the interface such as that shown in Fig.11. In the simulations, the interplanar spacing of each close packed planes was fixed at 0.2309 nm. This procedure necessarily means that $TiAl$ is assumed to have a cubic structure with $a=0.400$ nm instead of

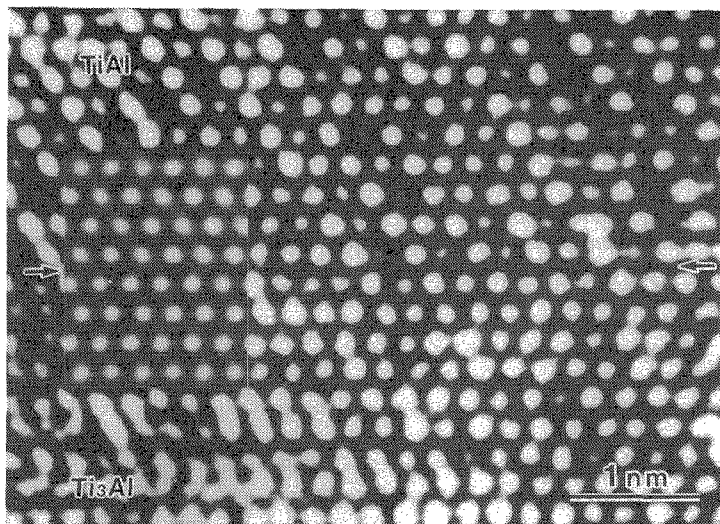


Fig.14 An enlargement of the framed part in Fig.10. The calculated image is inserted in the figure [11].

the tetragonal structure with $a=0.400$ nm and $c=0.406$ nm ($c/a=1.015$) and Ti_3Al to have a hexagonal structure with $a=0.5657$ nm and $c=0.4619$ nm ($c/a=0.817$) instead of that of $a=0.577$ nm and $c=0.462$ nm ($c/a=0.801$). The unit cell used in the simulations has the orthorhombic structure with $a=0.9798$ nm, $b=1.8475$ nm and $c=0.5657$ nm, containing 64 atoms. The calculated HREM images using the model interfaces shown in Figs.11(a) and (b) are shown in Figs.12 and 13, respectively. In Figs.12 and 13, the atomic positions are imaged as dark spots at the Scherzer defocus value (~ 40 nm) independent on crystal thickness and the contrast is reversed at the other defocus values used. At the defocus values other than the Scherzer, the atomic rows composed of Ti atoms only in the TiAl and Ti_3Al phases are imaged as the strongly bright spots over the wide range of crystal thickness as deduced in Figs.4 and 6. Thus, it is evident that the difference in the alignment of the atomic rows composed of Ti atoms only between the TiAl and Ti_3Al phases can be recognized in the HREM images as the difference in the alignment of the strongly bright spots.

Since it becomes clear that at certain values of defocus, the model interface of Fig.11(a) can be distinguished from that of Fig.11(b) in the HREM images, matching of the calculated images with the experimental images was undertaken and the result obtained is presented in Fig.14. Figure 14 shows the enlargement of the framed part in Fig.10. It is evident in the figure that the strongly bright spots corresponding to the atomic rows composed of Ti atoms only are aligned across the TiAl/ Ti_3Al interface. This indicates that the model interface shown in Fig.11(a), in which the atomic rows composed of Ti atoms only in TiAl and Ti_3Al are aligned across the interface, is more energetically favored than that shown in Fig.11(b) [11, 14]. The calculated HREM image using the model interface shown in Fig.11(a) is superimposed in the figure and a good matching is obtained between the experimental and calculated images. This result was obtained on all of the five $TiAl_{(11\bar{1}0)}/Ti_3Al_{(11\bar{2}0)}$ interfaces studied.

4. DISCUSSION

The five possible orientation relationships of the cases (b) and (c) in eq.(4) and of (a), (b) and (c) in eq.(5) have been found to occur between the two neighbouring TiAl ordered domains separated by the lamellar domain boundaries. However, in most cases, the two neighbouring domains are in the true-twin relation corresponding to the case (a) in eq.(5). This is because the lamellar domain boundaries of the true-twin-type have a much lower energy than those of the other types. In the following, energies of various TiAl/TiAl interfaces are estimated on the basis of a hard sphere model [3,12].

Let us consider an AB compound with the $L1_0$ structure. The energy of the true-twin type lamellar boundary, γ_T , considering the first- and second-nearest neighbour interactions only, is

$$\gamma_T = 2[\Phi_{AA}(r') + \Phi_{BB}(r')]/\sqrt{3}a^2 \quad \dots\dots (6)$$

where the slight tetragonality of the TiAl phase is neglected and $\Phi_{ij}(r')$ is the interaction energy between i and j atoms at the separation $r' = 2/\sqrt{3}a$ where a is the lattice parameter. γ_T is naturally one half that of the superlattice intrinsic stacking fault (SISF) which is given in [3]. Similarly, the energy, γ_R , of the 120° -rotational lamellar domain boundary corresponding to the cases (b) and (c) in eq.(4) is

$$\gamma_R = (2V^{(1)} - 6V^{(2)})/\sqrt{3}a^2 \quad \dots\dots (7)$$

where $V^{(k)} = (\Phi_{AA}^{(k)} + \Phi_{BB}^{(k)} - 2\Phi_{AB}^{(k)})/2$ and $\Phi_{ij}^{(k)}$ are the pairwise interaction energies between k th neighbour atoms. γ_R is one half that of antiphase boundary (APB) with a fault vector of $\frac{1}{2}\langle 10\bar{1} \rangle$ on (111) given in [3]. The energy of the $\frac{1}{2}\langle 10\bar{1} \rangle$ APB on {100} is

$$\gamma_{APB}^{(100)} = -4V^{(2)}/a^2 \quad \dots\dots (8)$$

Therefore, $V^{(2)} < 0$ as far as the $L1_0$ structure is stable. The energy, γ_P , of the pseudotwin-type lamellar boundary corresponding to the cases (b) and (c) in eq.(5) is

$$\begin{aligned} \gamma_P &= \gamma_P + [\Phi_{AA}(r') + \Phi_{BB}(r') + \Phi_{AB}(r')]/\sqrt{3}a^2 \\ &\simeq \gamma_R + \gamma_T. \end{aligned} \quad \dots\dots (9)$$

Equations (6) and (7) do not tell us which of γ_R and γ_T is larger. However, γ_{SISF} has been found to be much lower than $\gamma_{APB}^{(111)}$ not only through weak-beam TEM observations of superlattice dislocations in TiAl [15], but also through theoretical calculations of defect energies in TiAl using the FLAPW and LKKR methods [16,17]. The value of $\gamma_{APB}^{(111)}/\gamma_{SISF}$ are about 2 (experimental) and 6 (theoretical). Using these values of $\gamma_{APB}^{(111)}/\gamma_{SISF}$, the ratio of energies $\gamma_T : \gamma_P : \gamma_R$ can be estimated roughly to be 1 : 3 : 2 or 1 : 7 : 6. This clearly explains why the true-twin-type lamellar domain boundaries are observed in the TiAl phase much more frequently than those of the 120° -rotational- and the pseudotwin-types. The estimation of energies of those boundaries using many-body potentials of the Finis-Sinclair type is in progress.

5. CONCLUSIONS

The atomic structure of the lamellar boundaries in Ti-rich TiAl compounds was characterized by high-resolution electron microscopy coupled with computer simulation of HREM images. Interfaces between differently oriented TiAl domains are atomistically flat and in most cases, contain no Ti₃Al plates. Interfaces between TiAl and Ti₃Al are also atomistically flat and perfectly coherent although they contain some ledges. At interfaces between TiAl and Ti₃Al, the atomic rows composed of Ti atoms only are aligned across the interface between the two phases.

Acknowledgements

This work was supported by Grant-in-Aid for Scientific Research and Development from Ministry of Education, Japan and in part by The Iketani Science and Technology Foundation's Research Grant.

References

- [1] S.M.L. Sastry and H.A. Lipsitt, Titanium '80, Eds. H. Kimura and O. Izumi (The Metallurgical Society of AIME, Warrendale, 1980) p.1231.
- [2] M. Yamaguchi, S.R. Nishitani and Y. Shirai, High Temperature Aluminides and Intermetallics, Eds. S.H. Whang, C.T. Liu, D.P. Pope and J.O. Stiegler (The Minerals, Metals & Materials Society, Warrendale, 1990) p.63.
- [3] M. Yamaguchi and Y. Umakoshi, Prog. Mater. Sci., 34 (1991) 1.
- [4] Y.W. Kim, High-Temperature Ordered Intermetallic Alloys N, edited by L.A. Johnson, D.P. Pope and J.O. Stiegler (Materials Research Society, Pittsburgh, 1991), p.777.
- [5] D. Shechtman, M.J. Blackburn and H.A. Lipsitt, Metall. Trans., 5 (1974) 1373.
- [6] E.L. Hall and S.C. Huang, J. Mater. Res. 4 (1989) 595.
- [7] M.J. Blackburn, Technology and Application of Titanium, edited by R.T. Jaffee and N.E. Promisel (Pergamon, London, 1970), p.633.
- [8] C.R. Feng, D.J. Michel and C.R. Crowe, Scripta Metall., 22 (1988) 1481, *ibid.*, 23 (1989) 1135, Phil. Mag. Lett., 61 (1990) 95.
- [9] D.S. Schwartz and S.M.L. Sastry, Scripta Metall. 23 (1989) 1621.
- [10] Y.S. Yan and S.K. Wu, Scripta Metall. Mater., 24 (1990) 1801, *ibid.*, 25 (1991) 255.
- [11] H. Inui, A. Nakamura, M.H. Oh and M. Yamaguchi, Ultramicrosc., 39 (1991) 268.
- [12] H. Inui, M.H. Oh, A. Nakamura and M. Yamaguchi, Phil. Mag. A, to be published.
- [13] J.C.H. Spence, Experimental High-Resolution Electron Microscopy (Clarendon, Oxford, 1981).
- [14] G.J. Mahon and J.M. Howe, Metall. Trans. 21A (1990) 1655.
- [15] G. Hug, A. Loiseau and P. Veyssiere, Phil. Mag. A, 57 (1988), 499.
- [16] C.L. Fu and M.H. Yoo, Phil. Mag. Lett., 62 (1990) 159.
- [17] C. Woodward, J.M. MacLaren and S. Rao, High-Temperature Ordered Intermetallic Alloys N, edited by L.A. Johnson, D.P. Pope and J.O. Stiegler (Materials Research Society, Pittsburgh, 1991), p.125.